POLITECNICO
MILANO 1863

DIPARTIMENTO DI MECCANICA

mecc

Experimental observation of non-reciprocal band-gaps in a space-time modulated beam using a shunted piezoelectric array

J. Marconi, E. Riva,M. Di Ronco, G. Cazzulani, F. Braghin, and M. Ruzzene

This is a post-peer-review, pre-copyedit version of *Experimental Observation of Nonreciprocal Band Gaps in a Space-Time-Modulated Beam Using a Shunted Piezoelectric Array*, J. Marconi, E. Riva, M. Di Ronco, G. Cazzulani, F. Braghin, and M. Ruzzene, Phys. Rev. Applied **13**, 031001. The final authenticated version is available online at: https://doi.org/10.1103/PhysRevApplied.13.031001

© 2020 American Physical Society

This content is provided under CC BY-NC-ND 4.0 license

DIPARTIMENTO DI MECCANICA ■ POLITECNICO DI MILANO
via G. La Masa, 1 ■ 20156 Milano ■ EMAIL (PEC): pecmecc@cert.polimi.it
http://www.mecc.polimi.it
Rev. 0

Experimental observation of non-reciprocal band-gaps in a space-time modulated beam using a shunted piezoelectric array

J. Marconi,[1] E. Riva,[1,*] M. Di Ronco,[1] G. Cazzulani,[1] F. Braghin,[1] and M. Ruzzene[2]

[1] *Department of Mechanical Engineering, Politecnico di Milano, 20156, Italy*

[2] *Department of Mechanical Engineering, University of Colorado, Boulder, CO 80309, USA*

(Dated: March 9, 2020)

In this work we experimentally achieve 1 kHz-wide directional band-gaps for elastic waves spanning a frequency range from approximately 8 to 11 kHz. One-way propagation is induced by way of a periodic waveguide consisting of an aluminum beam partially covered by a tightly packed array of piezoelectric patches. The patches are connected to shunt circuits, where switches allow a periodic modulation in time of the beam properties. A travelling stiffness profile is imposed by phasing the modulation of each active element, inducing the propagation of a plane wave along the material and establishing unidirectional wave propagation at bandgap frequencies.

Nonreciprocal devices have been pursued in various research domains and physical platforms, including quantum [1], electromagnetic [2, 3], acoustic [4–6] and elastic [7–10] media. These devices exhibit different received-transmitted fields when source and detector are exchanged [11]. This opens new possibilities for the control of energy flow with unprecedented performance in communication systems [12], unidirectional insulators [13] and converters [14, 15], among others. Important contributions in the context of one-way phonon transport have been formulated by Fleury et. al. [16, 17], demonstrating directional wave manipulation in acoustic cyrculator devices. Also, elastic and acoustic directional waveguides have been conceived and physically realized, in analogy with the *Quantum Hall effect* (QHE), achieving back-scattering immune and one-way topological edge states [18–22]. Other approaches to nonreciprocity leverage nonlinear phenomena [23, 24], metastability [25], bifurcation and chaos [26] which are particularly attractive solutions due to the presence of solely passive elements. However, the exploitation of nonlinear dynamics usually requires high wave amplitudes, thus making the physical realization impractical for compact devices. An effective platform to break reciprocity is offered by space-time modulated systems [27, 28]. Notable recent examples have employed programmable magnetic lattice elements [29] and magnetic springs [30].

A number of papers have investigated meta-material control through electro-mechanical coupling, as described in the review paper [31]. In this work we experimentally investigate non-reciprocity in a electro-elastic beam, where spatial and temporal modulations are induced upon electric control of equivalent elastic properties. Namely, the spatial modulation is induced by bonding and array of piezoelectric elements on a passive substrate, which effectively alter the Young's modulus of the waveguide through negative capacitance shunts [32]. These are modulated in time through a switching logic, which enables the formation of a travelling stiffness profile that produces an asymmetric dispersion relation, a hallmark of non-reciprocity.

As shown in [32], the proposed platform effectively tests non-reciprocity of spatio-temporally modulated media, and may also be adopted to explore other phenomena associated with temporal and spatio-temporal modulation. Examples are parametric amplification [32], conversion [14], and topological edge-to-edge pumping [33, 34].

We consider the electro-mechanical beam illustrated in Fig. 1, which is made of an aluminum substrate having cross section $b \times H = 20$ mm $\times$ 1 mm and total length $L = 2400$ mm. An array of piezoelectric patches, separated by a 2 mm distance, is placed at $l_1 = 690$ mm and $l_2 = 1134$ mm from the left and right boundaries in order to minimize boundary reflections. For the same reason, the system is equipped with absorbing boundaries, obtained by covering the two clamped ends with mastic tape. The piezoelectric active domain is characterized by a length $l = 576$ mm and it consists of 24 pairs of patches ($\rho_p = 7.9$ kg/dm^3, $E_p = 62$ GPa) of size $b \times l_p \times h_p = 20 \times 22 \times 1$ mm, bonded on opposite surfaces. Each patch is connected to a shunt circuit emulating a series negative capacitance (NC), for a total of 48 shunts, which provide an effective stiffness reduction to the beam section when the circuit is closed [32]. Finally, a pair of patches bonded to the left end close to the clamp provide excitation.

A group of three patches pair defines a spatio-temporal (ST) cell, arranged in a configuration represented in Fig. 1b. The effective stiffness of each ST cell is modulated following the law $E_{s,k}(t) = E_{s,0}\left[1 + \alpha_m \mathrm{sign}\left(\cos\left(2\pi f_m t + (k-1)\pi/3\right)\right)\right]$, with $k = 1, 2, 3$ denoting the sub-cell number, while $\pi/3$ is the phase shift between the three consecutive active elements. Also, α_m defines the amplitude of modulation, and $f_m = 1/T_m$ is the modulation frequency, where T_m is the modulation period.

In the case at hand, the stiffness law is practically determined by the electrical boundary conditions of the piezoelectric patches according to the circuit schematic in Fig 1b. Periodically switching the NC circuits OFF and ON alternates the shunt impedance $Z^{SU}_{OFF} = 0$ and

* emanuele.riva@polimi.it

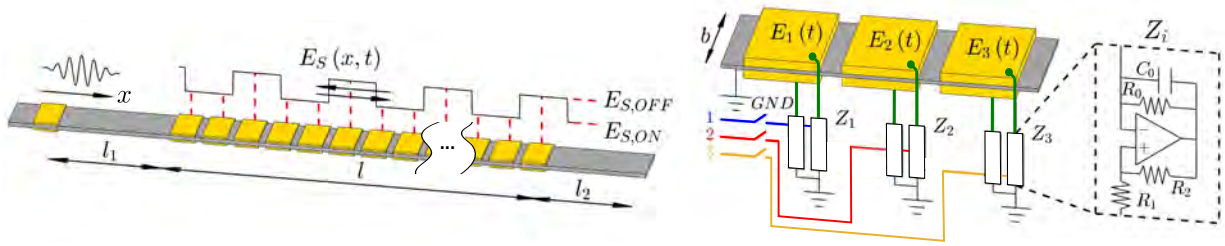

(a) (b)

FIG. 1: (a) Schematic of the electro-mechanical beam, showing the excitation patch providing the tone burst and the array of patches of the active domain (for convenience, only a portion of the beam is shown). (b) Close-in of the ST cell including the shunted series NC. High (low) stiffness is obtained by opening (closing) the switches connecting the power supply to the operational amplifiers. The first pair of patches of *each* ST cell is connected to switch 1 (blue wire), the second pair to switch 2 (red) and the third to switch 3 (yellow). Each *patch* is individually connected to a NC shunt circuit (green wires).

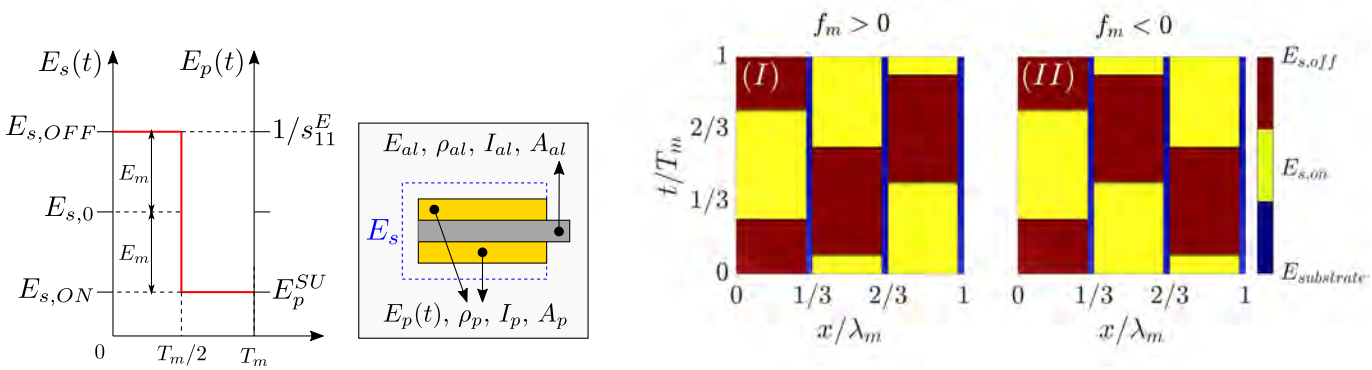

(a) (b)

FIG. 2: (a) Synoptic scheme and notation of stiffness for the patch (E_p), the sandwich (E_s) and of relevant modulation parameters. (b) Forward (I) and backward (II) Young's modulus profiles in the ST-cell domain D.

$Z_{ON}^{SU} = -\frac{1}{j\omega C_N}$, being $C_N = C_0 \frac{R_2}{R_1}$ the equivalent value of the synthetic NC shunt circuit under the assumption of infinite bias resistance R_0 [35, 36]. In practice, a finite value for R_0 is needed to ensure the correct operation of the shunt circuit. Once connected to the piezoelectric patch, the presence of R_0 affects the loss factor of the beam [37]. In the frequency range of interest, however, the circuit can be regarded as ideal (i.e. with $R_0 \to \infty$), as discussed in the Supplementary Material SM [38], where the stability analysis for the active NC shunts is also provided. As the stiffness of a shunted piezoelectric patch depends on the impedance of the shunt circuit, alternating the values Z_{OFF}^{SU} and Z_{ON}^{SU}, as described above, alternates the effective Young's moduli $E_p = 1/s_{11}^E$ (with s_{11}^E short-circuit mechanical compliance of the patch in 31-operation mode) and $E_p^{SU} = E_p \left(C_N - C_p^T\right) / \left(C_N - C_p^S\right)$ when the shunt is turned OFF and ON, respectively. Here, $C_p^{T(S)}$ is the piezo capacitance under stress (T) and strain (S) free conditions. The considered NC circuit data are listed in Tab. I. For more details on the computation of the equivalent piezo stiffnesses, refer again to SM. We now define $E_{s,ON/OFF}$ as biased and unbiased stiffnesses, which account for both piezo and substrate, as shown by the schematic in Fig. 2a. The latter allows to quantify the modulation parameter $\alpha_m = E_m/E_{s,0} = 27.5\%$, with $E_{s,0} = \left(E_{s,ON} + E_{s,OFF}\right)/2$ and $E_m = \left(E_{s,ON} - E_{s,OFF}\right)/2$. A travelling stiffness profile is obtained by phasing three spatially consecutive temporal modulation profiles. The

Name	Value	Units	Description
R_1	7.5	kΩ	–
R_2	13.7	kΩ	–
R_0	1000	kΩ	*bias resistance*
C_0	4.4	nF	*NC capacitance*
C_p	6.7–7	nF	*piezo patch capacity*
d_{31}	-1740	pm/V	*piezo strain coefficient*
k_{31}	0.351	–	*piezo coupling coefficient*

TABLE I: NC shunt circuit parameters.

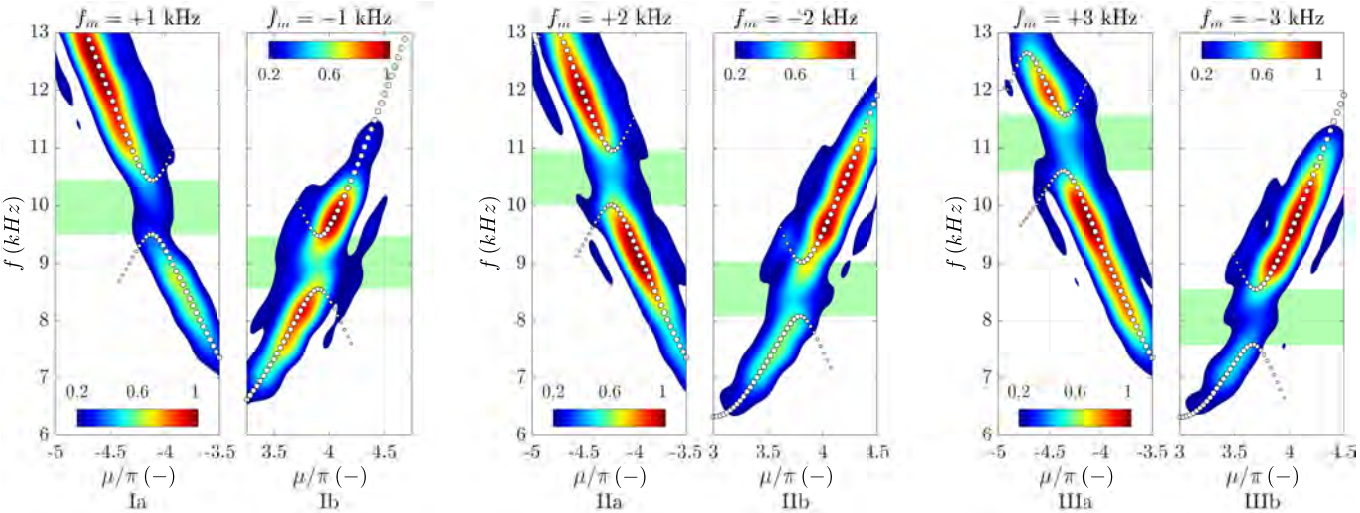

FIG. 3: Experimental (colored contours) and PWEM dispersion relations (white dots), for three levels of positive and negative switching frequencies. Experimental dispersion amplitudes are normalized by their respective maxima. On the background, directional bands as predicted by the PWEM are highlighted in light green.

ST unit cell effective stiffness, including active and passive sub-lattice elements is illustrated in Fig. 2b within the domain $D = [0, \lambda_m] \times [0, T_m]$, where λ_m is the spatial period. Forward (Fig. 2b$-I$) and backward (Fig. 2b$-II$) traveling modulations are achieved for $f_m > 0$ and $f_m < 0$, respectively. For convenience, in this work the excitation is fixed in space, therefore non-reciprocity is tested by simply changing the modulation speed from positive to negative. This is equivalent to keeping the sign of the modulation speed fixed, and moving the excitation source from one end to the other.

For each testing condition, the experimental dispersion relation is compared with the theoretical Bloch diagrams computed through the *Plane Wave Expansion Method* (PWEM). Timoshenko-beam model [39] is employed based on the governing equation for a beam:

$$\begin{aligned} (EI\alpha_x)_x + cAG\,(w_x - \alpha) &= (\rho I \alpha_t)_t \\ (cAG\,(w_x - \alpha))_x &= (\rho A w_t)_t \end{aligned} \tag{1}$$

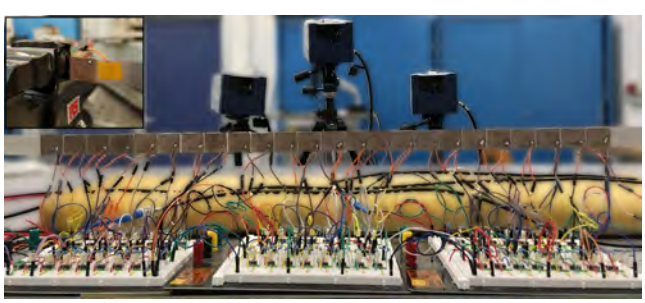

FIG. 4: Front view of the piezoelectric active domain with attached negative capacitance shunts. A *3D Scanner Laser Doppler Vibrometer (SLDV)* measures the velocity field along the beam.

where $(\cdot)_x = \partial(\cdot)/\partial x$ and $(\cdot)_t = \partial(\cdot)/\partial t$, w is the transverse displacement of the mid-surface, α is the cross sectional rotation of the beam, $c = 5/6$ is the shear correction coefficient, and G is the shear modulus. Given that, $EI\,(x,t)$, $cAG\,(x,t)$, $\rho I\,(x,t)$ and $\rho A\,(x,t)$ are periodic functions in space and time and can be expressed as Fourier series $C^{(k)} = \sum_{h,n=-\infty}^{+\infty} c_{h,n}^{(k)} \mathrm{e}^{\mathrm{i}(h\kappa_m x - n\omega_m t)}$ respectively, with $k = 1, ..., 4$, being $\kappa_m = 2\pi/\lambda_m$ the modulation wavenumber. In the current study, all inertial properties are constant in time. Ansatz solutions are sought as propagating waves along x, owning same periodicity of the modulation, therefore the out of plane displacement field $w\,(x,t)$ and the cross sectional rotation $\alpha\,(x,t)$ are approximated in terms of exponential wave functions $\alpha\,(x,t) = \sum_{p,q=-\infty}^{+\infty} a_{p,q} \mathrm{e}^{\mathrm{i}(p\kappa_m x - q\omega_m t)} \mathrm{e}^{\mathrm{i}(\kappa x - \omega t)}$ and $w\,(x,t) = \sum_{p,q=-\infty}^{+\infty} b_{p,q} \mathrm{e}^{\mathrm{i}(p\kappa_m x - q\omega_m t)} \mathrm{e}^{\mathrm{i}(\kappa x - \omega t)}$. Dispersion relations are then computed from a quadratic eigenvalue problem $\omega = \omega\,(\kappa)$ whose formulation is detailed in the supplementary material SM [38].

Figure 4 shows the experimental setup. Input waves are excited on the left side of the beam, in correspondence of the excitation piezo pair. An external trigger synchronously starts the acquisition system, the external excitation and the switches of the circuits, so that in each individual test the input wave always enters the array of patches finding the same phase of the stiffness modulation profile. The switches are controlled with a NI Compact-RIO and the acquisition is performed by a Polytec 3D *Scanner Laser Doppler Vibrometer* (SLDV) which measures the out of plane velocity field along the beam length.

Nonreciprocity is probed under two conditions. First, a tone burst excitation at frequencies centred in the bandgap is applied for analyzing positive and negative traveling modulations. Corresponding experimental

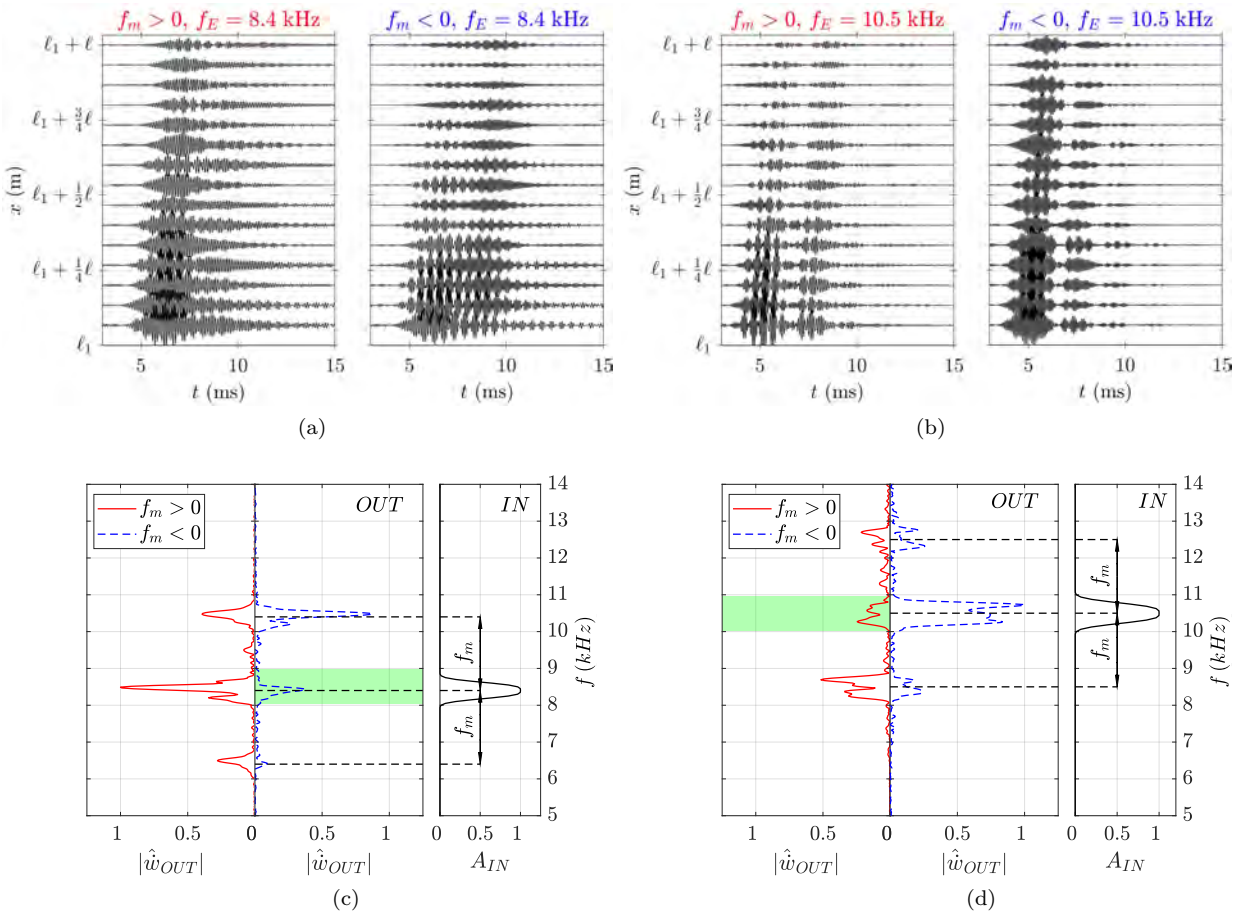

FIG. 5: (a) Velocity waterfall plots for a narrowband tone-burst at $f_E = 8.4$ kHz and of width $\Delta f_E = 0.8$ kHz, for $f_m = 2$ kHz > 0 (left) and $f_m = -2$ kHz < 0 (right). (c) Corresponding output spectra $|\hat{w}_{OUT}|$ of the wave exiting the final part of the periodic structure (at $x = l_1 + l$) and associated input spectrum. (b) Waterfall plots ($f_E = 10.5$ kHz, $\Delta f_E = 1$ kHz) for $f_m = 2$ kHz > 0 (left) and $f_m = -2$ kHz < 0 (right). (d) Output spectra $|\hat{w}_{OUT}|$ at $x = l_1 + l$ and associated input spectrum. For (a), data is normalized to the maximum amplitude between the two tests (same for (b) and for the output spectra in (c) and (d)).

dispersion relations are estimated by computing the 2D Fourier Transform of the measured velocity field within the domain of the structure. When $f_m = 0$, the space-only periodic medium supports a reciprocal bandgap (which is not present when all the patches are switched off) with a central frequency of $f_{BG} = 9.5$ kHz and amplitude $\Delta f \approx 1$ kHz. When the spatiotemporal modulation is turned on ($f_m > 0$), this bandgap moves to higher frequencies (Fig. 3 Ia-IIa-IIIa). For $f_m < 0$, opposite behavior is observed and the directional bandgap moves towards lower frequencies (Fig. 3 Ib-IIb-IIIb). Experimental data are in good agreement with the predicted analytic dispersion relation $\omega(\kappa)$, which is represented by the white dots, which confirms that the system operates as expected.

Finally, unidirectional attenuation levels are tested using a narrow-band excitation of spectrum centred at $f_E = 8.4$ kHz with $\Delta f_E = 0.8$ kHz, and modulation frequencies $f_m = \pm 2$ kHz. We measure the response at $x = l_1 + l$, that is just after the piezo array, which allows assessing the spectral content $\hat{w}_{OUT}(\omega)$ of the wave packet leaving the modulated domain. Specifically, for $f_m < 0$ wave propagation occurs with attenuation, as shown by the blue dashed curve in Fig. 5c. In contrast, a positive f_m leads to high amplitude propagating waves (red continuous curve). The measured velocity field is illustrated in Figs. 5a for $f_m > 0$ and $f_m < 0$, respectively. In the first case, the energy mainly propagates along the beam, while $f_m < 0$ leads to spatial attenuation through the periodic structure. Moreover, we observe a second wave packet, which is the back-reflected burst that undergoes a frequency conversion. This conversion appears in the frequency spectrum of the wave exiting the modulated beam (Fig. 5c), as some relevant component with associated frequency $f_E \pm f_m$ are present and can be generally associated

with Doppler-like effect in space-time modulated media [3, 14]. Analogous but reversed results are obtained when the tests are repeated with an input wave-packet centered at $f_E = 10.5$ kHz with $\Delta f_E = 1$ kHz (see Fig. 5d). Wave decay is observed for positive switching frequencies (red continuous curve), while for negative values propagation is allowed (blue dashed curve). Strong nonreciprocity and frequency conversion are also observable in Figs. 5b, demonstrating that elastic waves mainly propagate along the beam for $f_m < 0$.

In conclusion, this work experimentally investigates a modulated beam with space-time periodic properties and its ensuing non-reciprocal behavior. The modulation is produced through an array of piezo patches bonded to the beam, connected to switching negative shunting circuits. Breaking time invariance directional band-gaps and nonreciprocal behavior for propagating waves is observed, in a frequency range spanning from 8 kHz to 11 kHz.
The proposed setup may be easily integrated into micro electro-mechanical systems (MEMS), opening new possibilities for wave control in phononic communication devices. Moreover, the results suggest direct piezoelectric modulation as a viable platform for the investigation of a variety physical phenomena associated with time-varying media.

The Italian Ministry of Education, University and Research is acknowledged for the support provided through the Project "Department of Excellence LIS4.0 - Lightweight and Smart Structures for Industry 4.0".

[1] M. Z. Hasan and C. L. Kane, Colloquium: topological insulators, Reviews of modern physics **82**, 3045 (2010).
[2] A. B. Khanikaev, S. H. Mousavi, W.-K. Tse, M. Kargarian, A. H. MacDonald, and G. Shvets, Photonic topological insulators, Nature materials **12**, 233 (2013).
[3] N. Chamanara, S. Taravati, Z.-L. Deck-Léger, and C. Caloz, Optical isolation based on space-time engineered asymmetric photonic band gaps, Physical Review B **96**, 155409 (2017).
[4] S. A. Cummer, J. Christensen, and A. Alù, Controlling sound with acoustic metamaterials, Nature Reviews Materials **1**, 16001 (2016).
[5] J. Li, C. Shen, X. Zhu, Y. Xie, and S. A. Cummer, Nonreciprocal sound propagation in space-time modulated media, Physical Review B **99**, 144311 (2019).
[6] S. Karkar, E. De Bono, M. Collet, G. Matten, M. Ouisse, and E. Rivet, Broadband nonreciprocal acoustic propagation using programmable boundary conditions: From analytical modeling to experimental implementation, Physical Review Applied **12**, 054033 (2019).
[7] J. Vila, R. K. Pal, M. Ruzzene, and G. Trainiti, A bloch-based procedure for dispersion analysis of lattices with periodic time-varying properties, Journal of Sound and Vibration **406**, 363 (2017).
[8] H. Nassar, X. C. Xu, A. N. Norris, and G. L. Huang, Modulated phononic crystals: Non-reciprocal wave propagation and willis materials, Journal of the Mechanics and Physics of Solids **101**, 10 (2017).
[9] S. P. Wallen and M. R. Haberman, Nonreciprocal wave phenomena in spring-mass chains with effective stiffness modulation induced by geometric nonlinearity, Physical Review E **99**, 013001 (2019).
[10] E. Riva, M. Di Ronco, A. Elabd, G. Cazzulani, and F. Braghin, Non-reciprocal wave propagation in discretely modulated spatiotemporal plates, Journal of Sound and Vibration , 115186 (2020).
[11] C. Caloz, A. Alù, S. Tretyakov, D. Sounas, K. Achouri, and Z. L. Deck-Léger, Electromagnetic Nonreciprocity, Physical Review Applied **10**, 1 (2018).
[12] S. D. Huber, Topological mechanics, Nature Physics **12**, 621 (2016).
[13] G. Trainiti and M. Ruzzene, Non-reciprocal elastic wave propagation in spatiotemporal periodic structures, New Journal of Physics **18**, 083047 (2016).
[14] K. Yi, M. Collet, and S. Karkar, Reflection and transmission of waves incident on time-space modulated media, Physical Review B **98**, 054109 (2018).
[15] M. Oudich, Y. Deng, M. Tao, and Y. Jing, Space-time phononic crystals with anomalous topological edge states, Physical Review Research **1**, 033069 (2019).
[16] R. Fleury, D. L. Sounas, C. F. Sieck, M. R. Haberman, and A. Alù, Sound isolation and giant linear nonreciprocity in a compact acoustic circulator, Science **343**, 516 (2014).
[17] R. Fleury, D. L. Sounas, and A. Alù, Subwavelength ultrasonic circulator based on spatiotemporal modulation, Physical Review B **91**, 174306 (2015).
[18] A. B. Khanikaev, R. Fleury, S. H. Mousavi, and A. Alu, Topologically robust sound propagation in an angular-momentum-biased graphene-like resonator lattice, Nature communications **6**, 8260 (2015).
[19] H. Chen, L. Y. Yao, H. Nassar, and G. L. Huang, Mechanical quantum hall effect in time-modulated elastic materials, Physical Review Applied **11**, 044029 (2019).
[20] P. Wang, L. Lu, and K. Bertoldi, Topological phononic crystals with one-way elastic edge waves, Physical review letters **115**, 104302 (2015).
[21] X. Ni, C. He, X.-C. Sun, X.-p. Liu, M.-H. Lu, L. Feng, and Y.-F. Chen, Topologically protected one-way edge mode in networks of acoustic resonators with circulating air flow, New Journal of Physics **17**, 053016 (2015).
[22] L. M. Nash, D. Kleckner, A. Read, V. Vitelli, A. M. Turner, and W. T. M. Irvine, Topological mechanics of gyroscopic metamaterials, Proceedings of the National Academy of Sciences **112**, 14495 (2015).
[23] A. Mojahed, O. V. Gendelman, and A. F. Vakakis, Breather arrest, localization, and acoustic nonreciprocity in dissipative nonlinear lattices, The Journal of the Acoustical Society of America **146**, 826 (2019).
[24] M. D. Fronk, S. Tawfick, C. Daraio, S. Li, A. Vakakis, and M. J. Leamy, Acoustic non-reciprocity in lattices with nonlinearity, internal hierarchy, and asymmetry: Computational study, Journal of Vibration and Acoustics, Transactions of the ASME **141**, 1 (2019).

[25] Z. Wu, Y. Zheng, and K. W. Wang, Metastable modular metastructures for on-demand reconfiguration of band structures and nonreciprocal wave propagation, Physical Review E **97**, 022209 (2018).

[26] N. Boechler, G. Theocharis, and C. Daraio, Bifurcation-based acoustic switching and rectification, Nature materials **10**, 665 (2011).

[27] H. Nassar, H. Chen, A. N. Norris, M. R. Haberman, and G. Huang, Non-reciprocal wave propagation in modulated elastic metamaterials, Proceedings of the Royal Society A: Mathematical, Physical and Engineering Sciences **473**, 20170188 (2017).

[28] E. Riva, J. Marconi, G. Cazzulani, and F. Braghin, Generalized plane wave expansion method for non-reciprocal discretely modulated waveguides, Journal of Sound and Vibration **449**, 172 (2019).

[29] Y. Chen, X. Li, H. Nassar, A. N. Norris, C. Daraio, and G. Huang, Nonreciprocal wave propagation in a continuum-based metamaterial with space-time modulated resonators, Physical Review Applied **11**, 064052 (2019).

[30] Y. Wang, B. Yousefzadeh, H. Chen, H. Nassar, G. Huang, and C. Daraio, Observation of nonreciprocal wave propagation in a dynamic phononic lattice, Physical review letters **121**, 194301 (2018).

[31] M. Kadic, G. W. Milton, M. van Hecke, and M. Wegener, 3D metamaterials, Nature Reviews Physics **1**, 198 (2019).

[32] G. Trainiti, Y. Xia, J. Marconi, G. Cazzulani, A. Erturk, and M. Ruzzene, Time-periodic stiffness modulation in elastic metamaterials for selective wave filtering: Theory and experiment, Physical review letters **122**, 124301 (2019).

[33] Y. E. Kraus, Y. Lahini, Z. Ringel, M. Verbin, and O. Zilberberg, Topological states and adiabatic pumping in quasicrystals, Physical review letters **109**, 106402 (2012).

[34] I. H. Grinberg, M. Lin, C. Harris, W. A. Benalcazar, C. W. Peterson, T. L. Hughes, and G. Bahl, Robust temporal pumping in a magneto-mechanical topological insulator, Nature Communications **11**, 1 (2020).

[35] B. De Marneffe and A. Preumont, Vibration damping with negative capacitance shunts: theory and experiment, Smart Materials and Structures **17**, 035015 (2008).

[36] S. O. R. Moheimani and A. J. Fleming, *Piezoelectric transducers for vibration control and damping* (Springer Science & Business Media, 2006).

[37] F. Casadei, B. S. Beck, K. A. Cunefare, and M. Ruzzene, Vibration control of plates through hybrid configurations of periodic piezoelectric shunts, Journal of Intelligent Material Systems and Structures **23**, 1169 (2012).

[38] See supplemental material at [xxxx] for more details on the analytical procedure for the band diagram computation and additional experimental results.

[39] K. F. Graff, *Wave motion in elastic solids* (Courier Corporation, 2012).

[40] M. Berardengo, O. Thomas, C. Giraud-Audine, and S. Manzoni, Improved resistive shunt by means of negative capacitance: new circuit, performances and multimode control, Smart Materials and Structures **25**, 075033 (2016).

[41] N. W. Hagood and A. von Flotow, Damping of structural vibrations with piezoelectric materials and passive electrical networks, Journal of sound and vibration **146**, 243 (1991).

[42] Y. Y. Chen, G. L. Huang, and C. T. Sun, Band gap control in an active elastic metamaterial with negative capacitance piezoelectric shunting, Journal of Vibration and Acoustics **136** (2014).

[43] K. Yi, M. Collet, M. Ichchou, and L. Li, Flexural waves focusing through shunted piezoelectric patches, Smart Materials and Structures **25**, 075007 (2016).

[44] G. Hu, J. Xu, L. Tang, C. Lan, and R. Das, Tunable metamaterial beam using negative capacitor for local resonators coupling, Journal of Intelligent Material Systems and Structures , 1045389X19891575 (2019).